Faraday Discussions

Accepted Manuscript

Faraday Discussions

Royal Society of Chemistry

ROYAL SOCIETY OF CHEMISTRY

www.rsc.org/faraday_d

Journal Name

ARTICLE

Protein Detection Using Tunable Pores: Resistive Pulses and Current Rectification

Emma L. C. J. Blundell[a†], Laura J. Mayne[a†], Michael Lickorish[a], Steve D. R. Christie[a], Mark Platt[a]*

We present the first comparison between assays that use resistive pulses or rectification ratios on a tunable pore platform. We compare their ability quantify the cancer biomarker Vascular Endothelial Growth Factor (*VEGF*). The first assay measures the electrophoretic mobility of aptamer modified nanoparticles as they traverse the pore. By controlling the aptamer loading on the particles surface, and measuring the speed of each translocation event we are able to observe a change in velocity as low as 18 pM. A second non-particle assay exploits the current rectification properties of conical pores. We report the first use of Layer-by-Layer, (LbL) assembly of polyelectrolytes onto the surface of the polyurethane pore. The current rectification ratios demonstrate the presence of the polymers, producing pH and ionic strength dependent currents. The LbL allows the facile immobilisation of DNA aptamers onto the pore allowing a specific dose response to VEGF. Monitoring changes to the current rectification allows for a rapid detection of VEGF 5 pM. Each assay format offers advantages in their setup and ease of preparation but comparable sensitivities.

Introduction.

Interest in nanoscale channels within synthetic materials have grown over the last two decades[1–3]. These channel have applications in biosensing[4–6], materials characterisation[7,8], quantification of ligand-target interactions[9–11], drug delivery[12], and mimicking biological systems enabling, the study of ionic transport within confined geometries[13–16]. These nanopores have been created in a range of materials from graphene[17–20], polymers[21], silicon nitride[22] and glass[13,14,23,24]. The transport of the ions or analyte through the channel can by controlled by tuning the applied potential, pore wall charge, pore size, supporting electrolyte concentration and composition, with a further degree of selectivity by modifying the pore walls with selective ligands[25–27].

In addition to the pore properties, the translocation speed and frequency of materials such as small molecules, proteins or nanosized particles is also governed by the analyte size and charge[5,28–31], figure 1a. Nanopore sensors can be categorised into two general areas. Resistive Pulse Sensors, RPS, where the translocation of the analyte creates a characteristic change in resistivity within the pore, figure 1a-b, or

a. Department of Chemistry, Loughborough University, Loughborough, LE11 3TU, United Kingdom. Email: m.platt@lboro.ac.uk; Tel: +441509 222 573
† These authors contributed equally to the work.
Electronic Supplementary Information (ESI) available: [details of any supplementary information available should be included here]. See DOI: 10.1039/x0xx00000x

ARTICLE

current flux/ rectification studies that monitor current –voltage, *I-V*, and can be dominated by the charge on the pore wall to measure, figure 1c. The Flux of material through the pore is determined by the small and large pore geometries, d_s and d_l, pore length, *L*, and analyte charge. By controlling the aspect ratio of the pore, RPS has been used to measure analytes that range from single molecules, DNA, proteins, cellular vesicles to cells bacteria and viruses, detailed reviews on the types of analytes and applications can be found elsewhere[4,5,28,30].

We present a comparison between RPS and rectification ratios on a tunable pore platform. The pore is made of polyurethane, *PU*, allowing manipulation (stretching) in real time to suit the sample.[32] The pores are conical in shape and here typically d_s > 700 nm. In the first example we utilise an aptamer modified nanoparticle to detect Vascular Endothelial Growth Factor, *VEGF*. By measuring the translocation velocities of the aptamer modified particles the VEGF protein was detected down to 18 pM, equating to circa 10 proteins/ particle. In comparison a second strategy was tested by modifying the pores directly with the anti-VEGF aptamer and monitoring the current rectification ratio (measured at ±1.6V) in the presence of the VEGF protein. The surfaces of the pores were easily modified using a layer-by-layer, LbL, assembly of polymers, polyethylene amine, PEI, and polyacrylic acid-maleic acid, PAAMA. The use of PEI and PAAMA allowed for the easy modification, and reversible surface charge of the pores giving a pH and ionic strength controlled current flow, with current rectification ratios as high as 3. The LbL assembly was shown to be stable for days, allowing the modification of the pore wall with DNA via standard carbodiimide chemistry. The current rectification assay allows for the detection of VEGF down to 5 pM. Despite this comparable sensitivity, the RPS offers a larger dynamic range. The scope and ease of each assay format allows for a versatile technology that can be tailored to suite the target analyte.
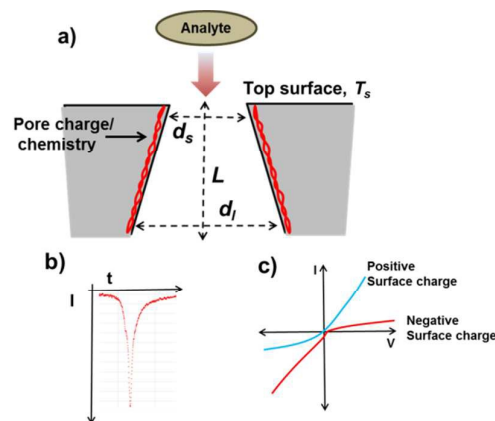

Figure 1. a) Schematic of a conical PU pore with small, large pore diameter and pore length, d_s, d_l and L respectively. The top surface of the pore is labelled T_s. b) Example of a resistive pulse. c) Schematic of I-V curves for conical pores with different surface charges.

Materials and methods.

Poly(ethyleneimine), PEI, low molecular weight, LMW (LMW PEI Mw ~ 2000 g mol^{-1}, 50 % wt., 408700) and high molecular weight, HMW, (HMW PEI Mw 750 000 g mol^{-1}, analytical standard, 50 % wt., P3143), poly(acrylic acid-co-maleic acid) (PAAMA, Mw ~3000 g mol^{-1} 50 % wt, 416053), phosphate buffered saline solution (P4417 (0.01 M phosphate buffer, 0.0027 M Potassium Chloride, 0.137M Sodium Chloride, pH 7.4)), bovine serum albumin (BSA, lyophilized powder, ≥96 %, A2153) and 2-(N-Morpholino)ethanesulfonic acid hydrate (MES hydrate, ≥99.5 %, M2933) fibrinogen from human plasma (F3879), albumin from human serum (A9511) and γ-globulin from human blood (G4386) were purchased from Sigma Aldrich, UK. Tunable conical pores (NP200) were purchased from Izon Science (Christchurch, NZ). Carboxylated polystyrene particles with a mean nominal diameter of 220 nm were purchased from Bangs Laboratories, US and are denoted as CPC200. Potassium chloride (KCl, >99 %, P/4240/60) and Potassium hydroxide (KOH, 0.1M, >85 %, P/5600/60) were purchased from Fisher Scientific, UK. Hydrochloric acid (HCl, 0.5M, 37 %) was purchased from VWR, UK. 1-ethyl-3-(3-dimethylaminopropyl)carbodiimide hydrochloride (EDC, 22980) and Recombinant Human Vascular

Endothelial Cell Growth Factor (VEGF, lyophilised, >95 %, PHC9394) were purchased from Thermo Scientific, UK. Streptavidin coated superparamagnetic particles (120 nm, 4352 pmol/mg binding capacity, 03121) were purchased from Ademtech, France. The custom DNA oligonucleotide

5'TGTGGGGGTGGACGGGCCGGGTAGATTTTT (V7t1 amine)[33], was purchased as a lyophilised powder (100 pmol/μL) from Sigma Aldrich, UK. The sequence was synthesised, with a biotin or amine functional group at the 3' end.

All reagents were used without further purification and all solutions were prepared in purified water with a resistance of 18.2 MΩ cm (TKA, Smart2Pure). pH of solutions were altered using HCl and KOH and the solutions were measured using a Mettler Toledo easy five pH meter with a Mettler Toledo InLab micro electrode.

Particle Assay

120 nm diameter streptavidin coated particles were diluted to a concentration of approximately 5×10^9 particles/mL. The diluted particle solutions were then vortexed for 30 s, and sonicated for 2 min, to ensure they were well dispersed. The biotinylated aptamer was added to the streptavidin coated particles (4352 pmol/mg binding capacity – determined by the supplier) at 113 and 226 nM for 50 and 100% DNA coverage per particle, respectively. The samples were then placed on a rotary wheel for 30 min. Any unbound DNA remaining in solution was then removed via magnetic separation by placing the samples onto a Magrack (GE Healthcare, UK) for 30 min. The supernatant was then removed and replaced with new buffer (PBS). The VEGF was added at the required concentration and then placed on a rotary wheel for 30 min before being analysed.

TRPS Set-Up

All measurements were conducted using the qNano (Izon Sciences Ltd, NZ) combining tunable nanopores with data capture and analysis software, Izon Control Suite v.3.2. The lower fluid cell contains the electrolyte (75 μL). The upper fluid cell contains 40 μL of sample (which was suspended in the electrolyte) an inherent

pressure on the system (47 Pa) was present when making a measurement. After each sample run, the system was washed by placing 40 μL of the run electrolyte into the upper fluid cell several times with various pressures applied to ensure there were no residual particles remaining and therefore no cross contamination between samples. The membranes are placed into jaws on the qNano instrument and are capable of being stretched[34]. The applied stretch is quantified by the distance between the jaws, with an upstretched distance being 42 mm, any values quoted below are the additional distances in mm applied to the membranes. Most experiments run at 45 mm. The pore diameters measured in the SEM and in the text were calculated from the current at 45 mm stretch.

Translocation Speed

The velocity of the particle was calculated by extracting the pulse width. Blockade duration events are recorded from the peak of the blockade back to the baseline current; the total time gives the blockade duration. Nine time points are recorded along the peak[29], relative to different positions within the pore and are denoted $T_{0.90}$, $T_{0.80}$, $T_{0.70}$ etc, here we use one measurement $1/T_{0.5}$ to represent the particles velocity.

Pore Modification

Conical pores were modified by incubating the pore in the polymer solution (5 % wt. in H2O) at a stretch of 45 mm for two hours, followed by rinsing the pores with deionised water. The pores were then incubated with second polymer layer 2 hours, again washed with deionised water. This process was repeated until the required number of layers was achieved.

Modification of PAAMA modified pores with DNA

The aptamer was dissolved in 100 mM MES buffer (pH 5.9) containing 1 mg.ml^{-1} EDC. The final concentration of the DNA was 220 nM. The pores were incubated with the DNA and EDC solution for 2 hours.

VEGF I-V assay

VEGF was suspended in PBS buffer to give the desired concentration. DNA modified pores were incubated in the VEGF solution, in each experiment the VEGF

solution was only placed on the side of the pore with the small pore opening D_s. When multiple solutions of different concentrations of VEGF were used the lowest concentration was measured first. The VEGF solution was in contact with the pore for 30 minutes with the pore being rinsed with water × 3, and PBS × 3 after each protein concentration. The current rectification property of the pore was then measured, in a range of KCl solutions starting with 5 nM first and working up to 50 mM. When a BSA control was used, 50 nM BSA was incubated first for 30 minutes, with the rectification properties being measured in KCl solutions before adding VEGF to the pore.

I-V Measurements

The pores were mounted between two fluid cells which contain an electrolyte solution. Current-voltage (I-V) curves were recorded using Izon control suite v3.2, the potential was stepped in 100 mV increments from +1.6 to -1.6 V and the resulting current measured.

Results and discussion

Assay 1 – Measuring translocation times from resistive pulses.

To facilitate sample handling and assay speed some RPS strategies have included nanomaterials by either immobilising the target analytes onto their surface facilitating an analyte induced aggregation[35,36], or measuring the particle translocation speed/ frequency upon the binding of the analyte[11,30,37–40]. With the charge of the particle being a contributing factor in pore translocation speed and frequency, the use of DNA modified materials, and pores, has become increasingly popular[11,30,41–43]. The polyanionic backbone of the DNA can enhance or determine the translocation speed/ direction and frequency of the current[28].

In the first assay format 120 nm particles were modified with a VEGF aptamer[33]. In two variations on this experiment different surface coverages of VEGF aptamer were used. In condition one the streptavidin binding sites on the particles are saturated with biotinylated aptamer (termed FC), in the second; circa half of binding sites (defined by the suppliers specifications) were filled with the aptamer (termed

HC). The change in translocation time relative to a particle that was not incubated with the protein, i.e. a Blank, is shown in figure 2. In previous work we have shown how the translocation velocity can be measured from the pulse width and then converted to zeta potentials using henry's Law[29]. The technique was able to distinguish between DNA coverage, in addition to length and structure i.e. ssDNA or dsDNA, on the particles surface, with the detection of dsDNA down to 10 nM LOD[29].
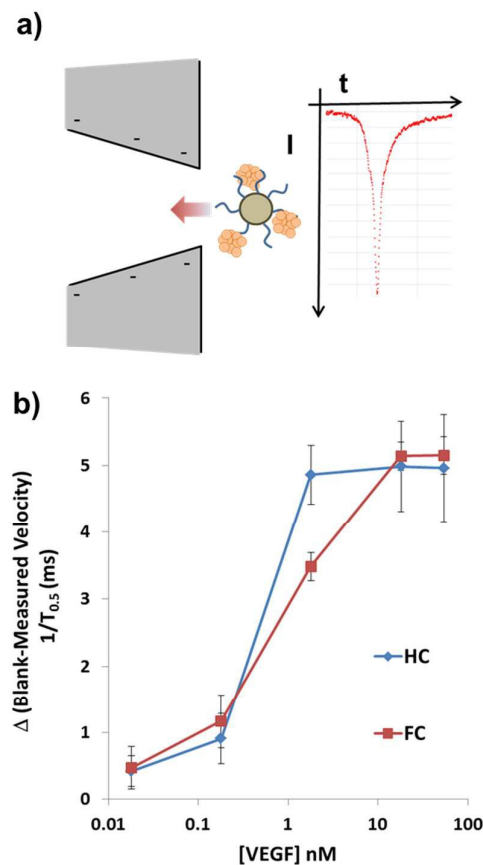
Figure 2. a) Schematic of the protein bound to the aptamer modified particle and typical resistive pulse. b) Plot of change in translocation time (relative to a blank = 0) versus VEGF concentration for aptamer modified beads, FC aptamer coverage – red, HC - blue circles. Each assay was run in triplicate with over 500 particles counted in each run.

In the strategy reported here rather than converting to zeta potentials, we simply measure changes to the relative velocities and infer the presence of the DNA and proteins. The hypothesis was that the binding of

the aptamer to the protein target, figure 2a, should result in a change in translocation time. Figure 2b shows the change in translocation times, relative to the blank, versus VEGF concentration for the two coverages of DNA.

There is a decrease in velocity for both sets of aptamer modified beads as the VEGF concentration increases. The change in aptamer shape from ssDNA to one of a folded tertiary structure upon binding the protein, bringing the DNA closer to the particles surface, could lead to a higher surface change density on the particle. This may result in an increase in particle speed. Conversely, as shown in figure 2b, a decrease in particle velocity upon the addition of the protein is observed. The velocity of the particles with HC remains constant at VEGF concentrations above 2 nM. This is attributed to the binding capacity of the beads being reached, and that any additional protein to the solution does not change the numbers on the particle surface, or if it does increase they cannot be measured via this technique. The velocity of the FC beads continues to decrease until a concentration of 18 nM is reached. By tuning the aptamer concentration on the particles surface the dynamic range of the assay can be extended.

The decrease in velocity is thought to be due several parameters that shield the negative charge on the phosphate backbone, increasing the counter ion condensation onto the DNA[43]. Firstly the conformation change to the DNA structure as it binds the protein requires an increased number of counter ions to stabilise the tertiary structure, and secondly the proteins pI is 8.5, and therefore is positively charged at the pH used in the experiment. Both particle assays see a decrease in speed, respective to their blanks, at a concentration of 18 pM.

Previous work using aptamer modified nanomaterials on the TRPS platform measured a change in particle translocation frequency as the transduction signal[11,39]. The benefit of the method presented here is in the ability to use data from each individual particle as they translocate the pore. Thus it does not rely upon averaging data across hundreds of particles/ min, reducing run times and bias in samples

with different particle concentrations. A potential limitation for future assays within complex biological solutions, is the tendency of proteins to foul the pore wall or particles surface. The particle translocation speed is a contribution of the electrophoretic speed of the particle and electroosmotic contribution of the pore wall. If the pore wall charge changes throughout the experiment it may impact on the assays reproducibility. A solution to this would be to develop a non-fouling coating on the particle and pore wall; preventing the nonspecific adsorption of proteins. Alternatively, the modification of the pore directly could facilitate the detection of the analyte of choice. Other nanopore systems have either utilised the natural surface functionality of the material or modified the pore walls with gold to allow the facile attachment of materials[44]. To date there has been no reported modification to the tunable polyurethane, PU, pores for RPS studies, although strategies for the modification of PU are available[45–47].

Assay 2 – Modification of the pore walls and current rectification

An alternative to a particle based assay is to use the change in ionic current through the pore, which can be controlled through electrostatic interactions via the pore wall. This effect is seen to a greater extent within conical pores, and typically recorded for pore openings where the diameter, D_s, is equivalent to the electrical double layer, DL, thickness,[24,48] although the DL does not need to fully extend across the pore opening[24], and larger pores exhibit current rectification effects[23,49]. Rectifying properties of conical pores are described in detail elsewhere[48], with the degree of rectification being defined as the ratio of absolute currents recorded at a given negative potential and the identical absolute positive potential. Typically conical pores with charged surfaces do not produce ohmic behaviour at lower electrolyte concentrations, and the magnitude of the current through the nanopore at negative potentials is greater or less than the current at positive potentials. The ratios can be tuned by changing the supporting electrolyte, pH, ionic strength and applied

ARTICLE

voltage, with the Current–Voltage, *I-V*, curves recording a preferred direction of current flow[24,48], figure 1c.

Tunable pores fabricated from PU have a small negative surface charge[29,49] at pH > 5, and are conical in shape. The unmodified pores used here had an approx. pore diameter, d_s, of 800 nm, at a stretch of 45mm, calculated from the measured current in 50 mM KCl. This is likely to be an averaged dimension, as in some instances the pore will not be spherical in shape, figure s1.

Figure 3a, black dashed line, shows the I-V curves of an unmodified pore in 5 mM KCl. A weak current rectification ratio of 1.38 is recorded. The I-V curve for an unmodified pore in 50 mM KCl is shown in figure 3b, and here the rectification value is 1, illustrating the return of the ohmic response at higher ionic strengths.
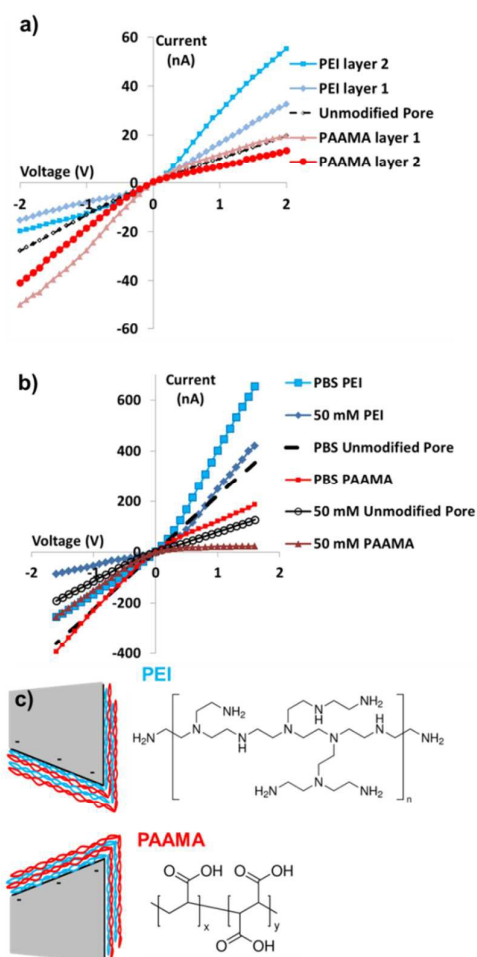

Figure 3. a) Current-Voltage curves for HMW PEI and PAAMA layers alongside a blank unmodified pore in 5 mM KCl. b) Current-Voltage curves for layer 2 bilayers alongside a blank unmodified pore. c) Schematic of the layer by layer assembly of PEI and PAAMA.

In an attempt to introduce a facile method for modifying the surface chemistry of the pore a layer-by-layer LbL, assembly using PEI/PAAMA was investigated. This system is well studied having been previously used to modify a range of materials[50–55]. We favoured this technique over other PU treatments such as plasma or the incorporation of grafting polymers into the matrix via swelling[47,56,57], as it allows for a simply and rapid dip coating strategy. In addition the LbL would allow the thickness and even the porosity of the PEI/PAAMA bilayer to be controlled in the future[53]. Here we have adopted to use a similar system as Yang et. al.[54] and Fu et. al.[53] that have shown how the thickness of the bilayers can be controlled ensuring that they do not extend across the pore opening and that the thickness of the bilayers remains in the order of a few nanometres.

Figure 3c, shows the schematic of the bilayer construction with consecutive PEI/ PAAMA layers. The resulting I-V curves in 5 mM KCl are shown in figure 3a alongside the unmodified pore. The addition of the PEI onto the pores surface resulted in a change in the preferred direction of current flow, with a reduced and enhanced current flow through the pore under a negative and positive applied potential respectively. This is indicative of a positive surface charge[58]. Upon coating with PAAMA, the surface charge switches to being negative, resulting in the preferred direction of current flow being inverted; figure 3a. All rectification ratios for the HMW PEI bilayers are listed in table 1, measured at ±1.6V. The additional of each layer of the LbL assembly caused the preferred current direction, or "on state" to be switched. The magnitude of the rectification can be used to access the presence and quality of the pore coating and as the number of bilayers increased the rectification ratios improved. It is interesting to note that even with two bilayers added to the pore walls, the pore opening remains unobstructed, as the additional of 210 nm particles to the upper fluid cell results in a standard resistive pulse response as they traverse the pore, data not shown.

Figure 3b shows the effect in increasing the ionic strength of the solution on the rectification ratio, again values are listed in table 1. Increasing the ionic strength reduced the rectification value, however it is interesting to note that even at >100mM KCl with a pore diameter circa 800nm some rectification was observed. The current rectification may have been enhanced by the nature of the modification of the pores here. The PU pores have a large area (circa diameter 2.5 mm) on the top surface, T_s, shown in figure 1. This surface is also modified along with the inner pore walls via the LbL route. A combination of top surface and pore wall modification has been shown to have a larger effect on the rectification ration[24].

A similar set of I-V curves were obtained using LMW PEI, shown in figure s2. However the rectification ratios for each subsequent PEI and PAAMA layer were smaller. This is likely due to the nature of the PEI layer placed onto the surface. The mechanism for LbL assembly goes through island formation before forming a full layer and it is hypothesised that when using the LMW PEI it takes longer to form a fully coated surface layer.

	Rectification Ratio				
[KCl] mM	Unmodified Pore	PEI - Layer 1	PAAMA - Layer 1	PEI - Layer 2	PAAMA - Layer 2
5	1.38	0.46	2.41	0.37	2.86
10	1.09	0.67	1.69	0.29	2.44
50	1.09	0.90	1.10	0.73	2.09
PBS (pH 7.4)	1.15	0.81	1.10	0.93	1.29

Table 1. Rectification ratios for pores measured in KCl solution circa pH 7. Listed in the rectification value of the same surface in 1 x PBS.

	Rectification Ratio	
pH	Unmodified Pore	PEI - Layer 2	PAAMA - Layer 2
3	0.83	0.31	0.73
7	1.40	0.52	1.98

Table 2. Rectification ratios for pores with different surface chemistry as a function of pH. The concentration of KCl was 5 mM for all experiments. HMW-PEI was used for the bilayers.
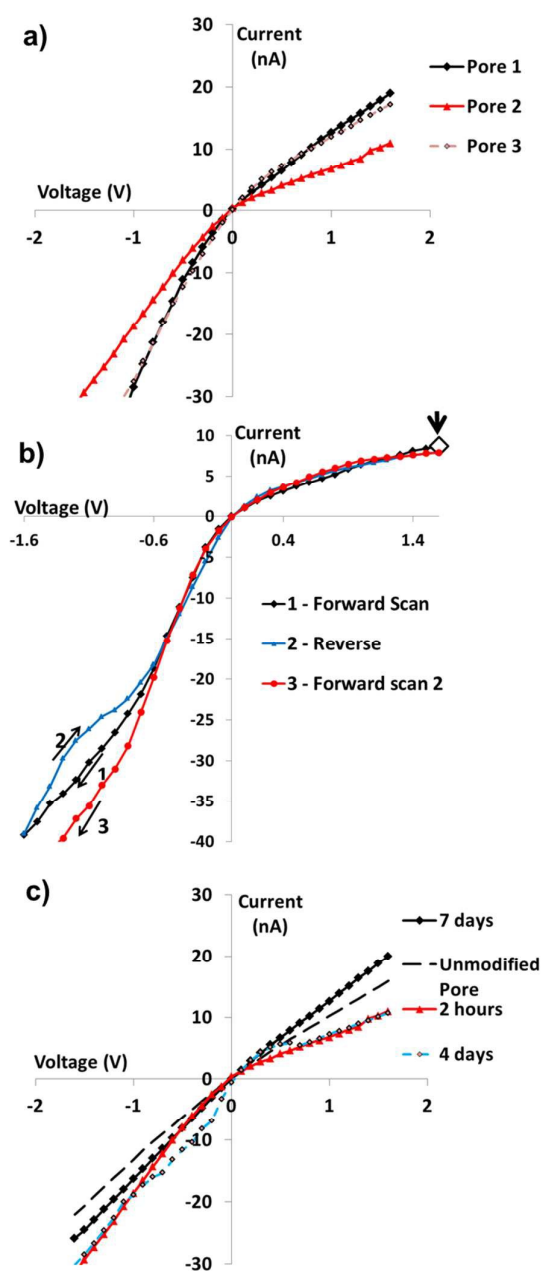

Figure 4. a) I-V curves for three different NP200 pores coated with two bilayers. b) Consecutive scans across the voltage range starting point is indicated with an arrow. Forward scan refers to moving from +1.6V to -1.6V. Each current was recorded after a 5 second wait to the new voltage. c) I-V curves for an individual pore coated with two bilayers, each day the pore was set up and I-V curves recorded before being washed with DI water and air dried. All data obtained at 45 mm Stretch, pH 6.8 and 5 mM KCl.

The LbL approach was reproducible on multiple pores, figure 4a, and shows little hysteresis through multiple cycles shown in figure 4b. The LbL coating was

ARTICLE

also stable over short periods of time even after multiple uses, washes, and being dried and stored overnight, shown in figure 4c. Although multiple uses and storage for over a week resulted in a deterioration of the surface chemistry, figure 4c. The same pore could however be reused and recoated with comparable results, data shown in figure s3.

Given the flexible nature of the PU pore it should be possible to change the rectification ratio by stretching the pore with a smaller stretch producing a higher rectification ratio. Figure 5a shows the effect on the I-V curves as the stretch is decreased from 5 to 2 mm. As the pore opening, d_s, is reduced the observed current at positive potentials decreases. In addition to the pore size, both the PEI and PAAMA have functional groups that should allow a pH controlled current flow. Figure 5b and c shows the effect of pH on the I-V relationship for both the PEI and PAAMA surfaces, for comparison the data for an unmodified pore is given alongside. Lowering the pH of the solution to 3 increases the charge density on the PEI surface as more amines become protonated; this results in an increased current flow at positive potentials and a rectification ratio as low as 0.31. Conversely increasing the pH to 7 reduced the positive charge on the PEI and the current rectification ratio increases to 0.52. Table 2 lists the rectification ratios for PEI and PAAMA pores at pH 3 and 7. For the PAAMA surface at pH 3, the charge density across the carboxyl groups is reduced and the response is similar to the unmodified pore is recorded, table 2. Increasing the pH to 7 for the PAAMA pores increases the negative charge density of the PAAMA pore wall, with an observed decrease in current flow at positive potentials and a current rectification of 1.98. The unmodified pore shows a current rectification of 0.8 at a pH of 3, indicating the surface groups have become protonated.
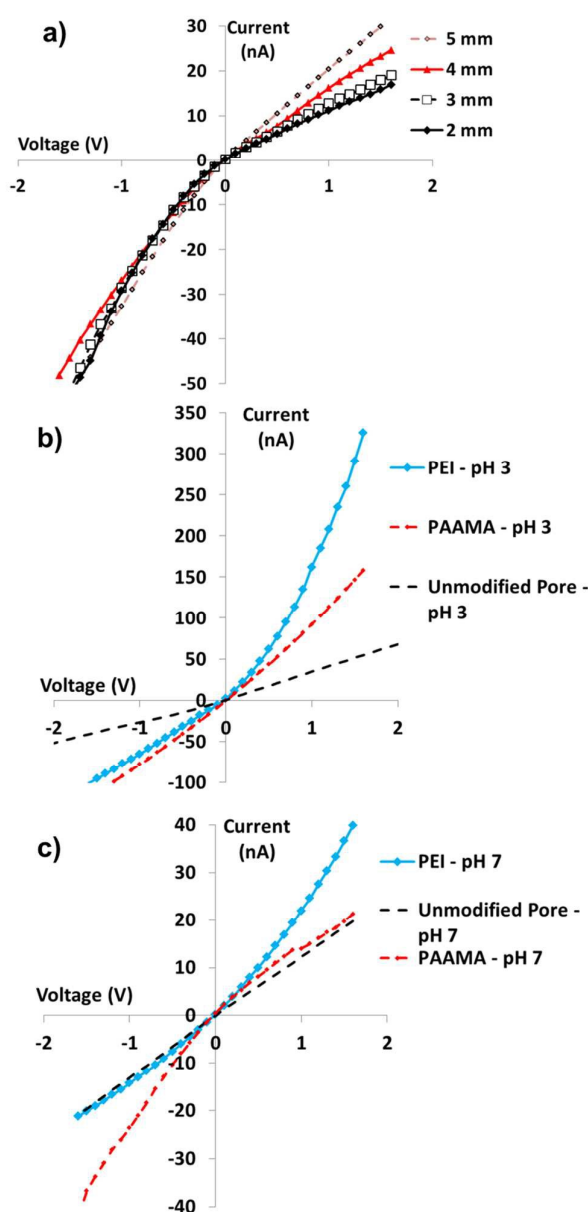

Figure 5. a) *I-V curves for a NP200 pore coated with two bilayers. Measured at, pH 6.8 and 5 mM KCl. b) I-V curves for a unmodified pore, a PAAMA (two complete bilayers) and PEI (1.5 bilayers). Obtained at 45 mm Stretch, pH 3 and 5 mM KCl. b) I-V curves for a unmodified pore, a PAAMA (two complete bilayers) and PEI (1.5 bilayers). Obtained at 45 mm Stretch, pH 7 and 5 mM KCl.*

For all pores a 210 nm diameter particle suspended in PBS was passed through the opening as we built up the layers. The particles ability to traverse the opening was interpreted to mean that the pore remained unblocked with a thick bilayer mesh, or that the bilayers have not restricted the pore orifice to a large extend.

The current flow through the pore has two contributing factors; the electroosmotic flow, EOF, across the pore surface and migration of ions through the centre. Whilst others have shown the EOF to be a small contributing factor to current rectification in smaller pores[24], and that a combined effect of the charge on the pore wall and top surface, has the largest contribution to the current rectification [24]. In the work reported here a large area of T_s is also modified with the bilayers and future work may be needed to ascertain if this has a larger contribution in the PU pores. The observation of rectification behaviour does illustrate that the enriched ion zone at the pore mouth used to describe the rectification properties of smaller pores[24,42] sufficiently exerts an influence across the larger opening, even when the electrical DL is much shorter than the opening D_s. This effect has also been attributed to biphasic pulse behaviour in TRPS[49].

The reported setup allows for the easy modification of the pore wall, and by using different polymers or different thickness it may be possible to further tune these larger pores to be ion selective.

Modification of the Pore walls with ssDNA

The main motivation for modifying the pore walls with the LbL polymers was to introduce a functionality to which biomolecules could be easily coupled to the pore wall. Similar aspirations have led to the modification of pores with Au allowing thiol terminated ligands to be placed along the pore wall or the utilisation of the carboxyl groups[43,59]. Our method of immobilisation uses EDC chemistry placing the DNA across the T_s and pore surface, shown schematically in figure 6a. Figure 6b shows the I-V plots for a pore having gone through the LbL and DNA assembly, a magnified section through the origin is given in figure 6c. In the case were DNA was immobilised onto the pore wall only one bilayer was used. The reason being that one bilayer was sufficient to introduce the carboxyl groups on the surface, and stopping at one bilayer reduced the number of preparation stages. The data is figure 6 was recorded at 50 mM KCl. At higher ionic strengths, >50 mM KCl, the DNA modified pores do not exhibit current rectification, equivalent 5 mM KCl curves are given in

figure s4. The reduction in rectification for the DNA surface over the PAAMA layer may be due to the high number of DNA strands on the pores surface and the counter ion condensation shielding the high charge densities; in addition the EDC chemistry may have cross linked the PAAMA to the underlying PEI causing a reduction in surface charge density.
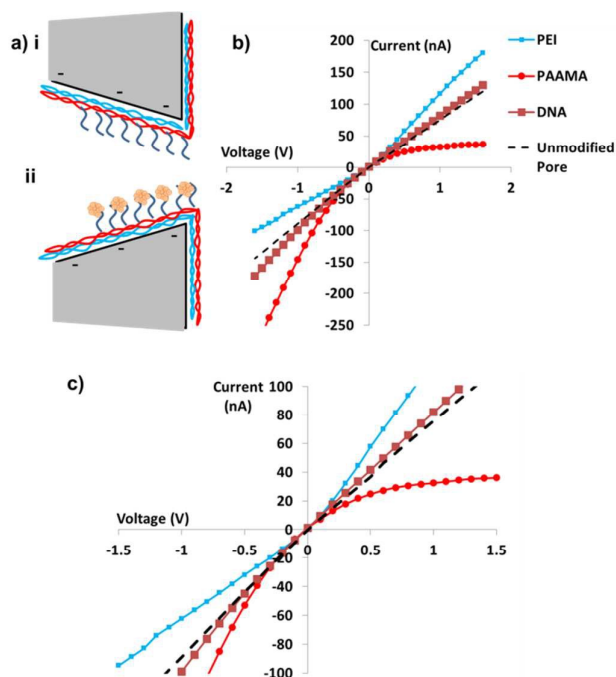

Figure 6 ai) Schematic of the DNA modified pore and ii) aptamer-VEGF interaction. b) I-V curves for each layer in the DNA immobilisation. c) Enlarged section of b. All data recorded at 50 mM KCl, pH 6.8, 45 mm stretch.

Incubation of the pore with the target VEGF results in a strong rectification; shown in figure 7a (equivalent data for 5 mM KCl are given in figure s5). The decrease in currents at positive potentials was shown to be specific to the aptamer-VEGF interaction in the presence of BSA (figure s6), figure 7b and a mixture of other proteins whose pI values range from 5-7, figure s7.

A similar trend in rectification properties was observed for the Lysozyme system in cylindrical pores[59], the explanation given for the behaviour was attributed to the proteins high pI, and the binding of the protein to the DNA inverting the surface charge. This resulted in a positive surface on one side of the

ARTICLE

pore and the asymmetric surface charge resulted in the current rectification. Our experiment may have produce a similar effect, i.e. the introduction of the protein on one side of the pore produced a different surface charge density from top to bottom. However if in our study this resulted in a positively charged narrow pore opening, studies into diode like conical pores would suggest the rectification properties would produce the opposite of the observed effects i.e. an increase in current at positive potentials[60], which is not the observed result.

conductivity at the pore mouth for positive potentials as described elsewhere[24].

Figure 8 shows the concentration dose response of the DNA modified pore at 50 mM KCl, equivalent 5 mM curves are show in figure s8. As the concentration of VEGF is increased the current measured at 1.6V decreases, and appears to saturate or remain unchanged beyond 5nM. The rectification ratios for the 50 mM KCl experiment are given in table 3. The detection of the VEGF at such low levels, when compared to RPS, may be aided by the inherent nature of the membrane to pre-concentrate cations in the pore mouth.
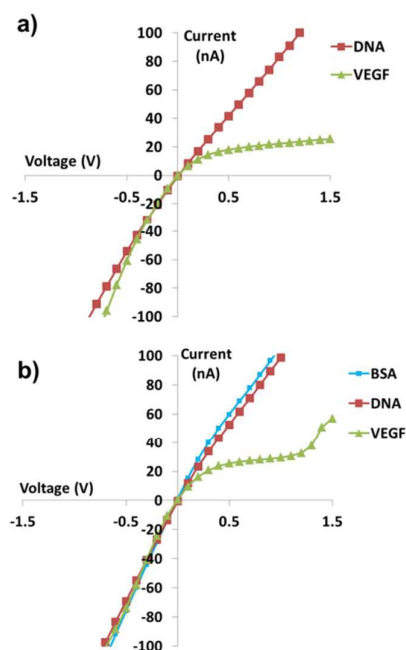

Figure 7 a) I-V curves for aptamer (DNA) and VEGF incubated pore. VEGF was 50nM. b) Equivalent data set for conditions given in a, for a second pore. The pore was first incubated with BSA at 50nM. KCl is 50 mM, Stretch – 45mm.

Our hypothesis for the observed rectification behaviour also relies upon the high pI of VEGF (8.2), and that the protein is positively charged. The inclusion of the protein to the DNA at the pore mouth and T_s increases the cation cloud density at the pore mouth. In additional to this the folding of the aptamer into a tertiary structure to bind to the VEGF must require an increase in counter ions to stabilise the structure, and these two factors contribute to a decrease in
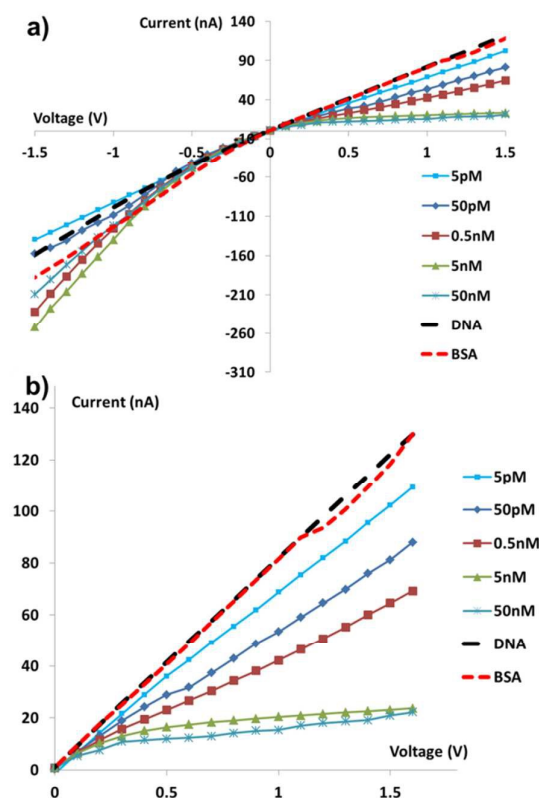

Figure 8 a) Plot of rectification ratio versus VEGF concentration for a third pore. b) magnified section of the current between 0-1.6 V. KCl 50 mM, pH 6.8. Stretch 45mm.Each measurement was taken in series on the same pore.

Concentraion of VEGF	Rectification ratio
5 pM	1.36
50 pM	1.93
0.5 nM	3.64
5 nM	11.60
50 nM	10.12
DNA	1.33
BSA	1.53

Table 3 Rectification ratios measured for the data shown in figure 8.

Conclusions

Presented is a comparison between a resistive pulse and current rectification aptamer assays using the same technology platform. To enable this we present the first LbL modification of PU pores that allows a pH, and ionic strength controlled current flow. We feel that the tunable pore is unique in this ability to be easily adapted to both, and that the LbL assay reported here offers a simple and reusable method for modifying the surface chemistry of the pores. The RPS assay offers a format that can be easily prepared and multiplexed by pairing each target with a unique particle size/ shape. Whilst it offers a wider dynamic range, its sensitivity is limited by number of proteins required to change the particle surface charge sufficiently to detect a measurable change in translocation velocity. Further improvement to the sensitivity may require the specific design of the particle size and surface to allow a limited and controlled number of aptamers, although this offers a complication in assay time as the flux of material through the pore decreases with smaller particles and pores, or the use of Janus particles to localise the biorecognition[35].

The LbL assembly of the pore offers a pH and ionic strength dependent rectification behaviour and is the first reported method on such a system. It allows the first observation of strong rectification on pores of this dimension. The strong rectifying properties illustrate that the electric double layer does not need to significantly extend across the pore opening, although it is acknowledged that further studies are required to access the effects of the modification of the top surface of the pore has on the rectification mechanism, and the total contrition of electroosmotic flow in these systems.

Notes and references

1 C. Dekker, *Nat Nano*, 2007, **2**, 209–215.

2 D. Branton, D. W. Deamer, A. Marziali, H. Bayley, S. A. Benner, T. Butler, M. Di Ventra, S. Garaj, A. Hibbs, X. Huang, S. B. Jovanovich, P. S. Krstic, S. Lindsay, X. S. Ling, C. H. Mastrangelo, A. Meller, J. S. Oliver, Y. V Pershin, J. M. Ramsey, R. Riehn, G. V Soni, V. Tabard-Cossa, M. Wanunu, M. Wiggin and J. A. Schloss, *Nat Biotech*, 2008, **26**, 1146–1153.

3 L. T. Sexton, L. P. Horne and C. R. Martin, *Mol. Biosyst.*, 2007, **3**, 667–685.

4 L. Sexton, L. Horne and C. Martin, in *Molecular- and Nano-Tubes SE - 6*, eds. O. Hayden and K. Nielsch, Springer US, 2011, pp. 165–207.

5 H. Bayley and C. R. Martin, *Chem. Rev.*, 2000, **100**, 2575–2594.

6 H. Bayley and P. S. Cremer, *Nature*, 2001, **413**, 226–230.

7 D. Kozak, W. Anderson, R. Vogel and M. Trau, *Nano Today*, **6**, 531–545.

8 G. S. Roberts, S. Yu, Q. Zeng, L. C. L. Chan, W. Anderson, A. H. Colby, M. W. Grinstaff, S. Reid and R. Vogel, *Biosens. Bioelectron.*, 2011.

9 P. Kohli, C. C. Harrell, Z. Cao, R. Gasparac, W. Tan and C. R. Martin, *Science (80-.).*, 2004, **305**, 984–986.

10 K. B. Jirage, J. C. Hulteen and C. R. Martin, *Science (80-.).*, 1997, **278**, 655–658.

Faraday Discussions Accepted Manuscript

ARTICLE

Journal Name

11   E. R. Billinge, M. Broom and M. Platt, *Anal. Chem.*, 2014, **86**, 1030–7.

12   P. M. S. and G. V. and S. S. and X. L. and M. Ferrari, *Nanotechnology*, 2004, **15**, S585.

13   W.-J. Lan, D. A. Holden, J. Liu and H. S. White, *J. Phys. Chem. C*, 2011, **115**, 18445–18452.

14   W.-J. Lan, D. A. Holden, B. Zhang and H. S. White, *Anal. Chem.*, 2011, **83**, 3840–3847.

15   K. A. Whitehead, R. Langer and D. G. Anderson, *Nat Rev Drug Discov*, 2009, **8**, 129–138.

16   S. Lee, Y. Zhang, H. S. White, C. C. Harrell and C. R. Martin, *Anal. Chem.*, 2004, **76**, 6108–6115.

17   S. Nam, I. Choi, C. Fu, K. Kim, S. Hong, Y. Choi, A. Zettl and L. P. Lee, *Nano Lett.*, 2014, **14**, 5584–5589.

18   R. R. Henriquez, T. Ito, L. Sun and R. M. Crooks, *Analyst*, 2004, **129**, 478–482.

19   T. Ito, L. Sun, R. R. Henriquez and R. M. Crooks, *Acc. Chem. Res.*, 2004, **37**, 937–945.

20   L. Sun and R. M. Crooks, *J. Am. Chem. Soc.*, 2000, **122**, 12340–12345.

21   G. S. Roberts, D. Kozak, W. Anderson, M. F. Broom, R. Vogel and M. Trau, *Small*, 2010, **6**, 2653–2658.

22   J. B. Heng, A. Aksimentiev, C. Ho, P. Marks, Y. V Grinkova, S. Sligar, K. Schulten and G. Timp, *Biophys. J.*, 2006, **90**, 1098–1106.

23   W.-J. Lan, C. Kubeil, J.-W. Xiong, A. Bund and H. S. White, *J. Phys. Chem. C*, 2014, **118**, 2726–2734.

24   H. S. White and A. Bund, *Langmuir*, 2008, **24**, 2212–2218.

25   E. A. Heins, Z. S. Siwy, L. A. Baker and C. R. Martin, *Nano Lett.*, 2005, **5**, 1824–1829.

26   Z. Siwy, L. Trofin, P. Kohli, L. A. Baker, C. Trautmann and C. R. Martin, *J. Am. Chem. Soc.*, 2005, **127**, 5000–5001.

27   M. Ali, P. Ramirez, M. N. Tahir, S. Mafe, Z. Siwy, R. Neumann, W. Tremel and W. Ensinger, *Nanoscale*, 2011, **3**, 1894–1903.

28   E. L. C. J. Blundell, L. J. Mayne, E. R. Billinge and M. Platt, *Anal. Methods*, 2015.

29   E. L. C. J. Blundell, R. Vogel and M. Platt, *Langmuir*, 2016, **32**, 1082–1090.

30   E. Weatherall and G. R. Willmott, *Analyst*, 2015, **140**, 3318–3334.

31   Y. Qiu, C. Yang, P. Hinkle, I. V Vlassiouk and Z. S. Siwy, *Anal. Chem.*, 2015, **87**, 8517–8523.

32   G. R. Willmott, R. Vogel, S. S. C. Yu, L. G. Groenewegen, G. S. Roberts, D. Kozak, W. Anderson and M. Trau, *J. Phys. Condens. Matter*, 2010, **22**, 454116.

33   Y. Nonaka, K. Sode and K. Ikebukuro, *Molecules*, 2010, **15**, 215–25.

34   R. Vogel, W. Anderson, J. Eldridge, B. Glossop and G. Willmott, *Anal. Chem.*, 2012, **84**, 3125–31.

35   M. Platt, G. R. Willmott and G. U. Lee, *Small*, 2012, **8**, 2436–2444.

36   Y. S. Ang and L. Y. L. Yung, *ACS Nano*, 2012, **6**, 8815–8823.

37   E. R. Billinge, J. Muzard and M. Platt, *Nanomater. Nanosci.*, 2013, **1**, 1.

38   E. R. Billinge and M. Platt, *Anal. Methods*, 2015, **7**, 8534–8538.

39   E. R. Billinge and M. Platt, *Biosens. Bioelectron.*, 2015, **68**, 741–748.

40   O. a Alsager, S. Kumar, G. R. Willmott, K. P. McNatty and J. M. Hodgkiss, *Biosens. Bioelectron.*, 2014, **57**, 262–8.

41   C. C. Harrell, P. Kohli, Z. Siwy and C. R. Martin, *J. Am. Chem. Soc.*, 2004, **126**, 15646–15647.

42   S. F. Buchsbaum, G. Nguyen, S. Howorka and Z. S. Siwy, *J. Am. Chem. Soc.*, 2014, **136**, 9902–9905.

43   G. Nguyen, S. Howorka and Z. S. Siwy, *J. Membr. Biol.*, 2011, **239**, 105–113.

44   M. Ali, S. Nasir, Q. H. Nguyen, J. K. Sahoo, M. N. Tahir, W. Tremel and W. Ensinger, *J. Am. Chem. Soc.*, 2011, **133**, 17307–17314.

45   L. Maisonneuve, O. Lamarzelle, E. Rix, E. Grau and H. Cramail, *Chem. Rev.*, 2015, **115**, 12407–12439.

46   F. Hileman, R. Sievers, G. Hess and W. Ross, *Anal. Chem.*, 1973, **45**, 1126–1130.

47   A. Kulkarni, W. Diehl-Jones, S. Ghanbar and S. Liu, *J. Biomater. Appl.* , 2014, **29** , 278–290.

48   Z. S. Siwy, *Adv. Funct. Mater.*, 2006, **16**, 735–746.

49   E. Weatherall and G. R. Willmott, *J. Phys. Chem. B*, 2015, **119**, 5328–5335.

50   B. Steitz, H. Hofmann, S. W. Kamau, P. O. Hassa, M. O. Hottiger, B. von Rechenberg, M. Hofmann-Amtenbrink and A. Petri-Fink, *J. Magn. Magn. Mater.*, 2007, **311**, 300–305.

51   J. J. O'Mahony, M. Platt, D. Kilinc and G. Lee, *Langmuir*, 2013, **29**, 2546–2553.

52   Y.-H. Yang, M. Haile, Y. T. Park, F. A. Malek and J. C. Grunlan, *Macromolecules*, 2011, **44**, 1450–1459.

53   J. Fu, J. Ji, L. Shen, A. Küller, A. Rosenhahn, J. Shen and M. Grunze, *Langmuir*, 2009, **25**, 672–675.

54   Y.-H. Yang, L. Bolling, M. Haile and J. C. Grunlan, *RSC Adv.*, 2012, **2**, 12355–12363.

55   P. Podsiadlo, M. Michel, J. Lee, E. Verploegen, N. Wong Shi Kam, V. Ball, J. Lee, Y. Qi, A. J. Hart, P. T. Hammond and N. A. Kotov, *Nano Lett.*, 2008, **8**, 1762–1770.

56   A. B. Jozwiak, C. M. Kielty and R. A. Black, *J. Mater. Chem.*, 2008, **18**, 2240–2248.

57   M. Gultekinoglu, Y. Tunc Sarisozen, C. Erdogdu, M. Sagiroglu, E. A. Aksoy, Y. J. Oh, P. Hinterdorfer and K. Ulubayram, *Acta Biomater.*, 2015, **21**, 44–54.

58   Z. Siwy, E. Heins, C. C. Harrell, P. Kohli and C. R. Martin, *J. Am. Chem. Soc.*, 2004, **126**, 10850–10851.

59   M. Ali, S. Nasir and W. Ensinger, *Chem. Commun.*, 2015, **51**, 3454–3457.

60   I. Vlassiouk and Z. S. Siwy, *Nano Lett.*, 2007, **7**, 552–556.

Faraday Discussions Accepted Manuscript